Detecting Subtle Seasonal Transitions of Upwelling in North-Central Chile

DAVID A. RAHN

Atmospheric Science Program, Department of Geography, University of Kansas, Lawrence, Kansas

BENJAMÍN ROSENBLÜTH*

Departamento de Geofísica, Facultad de Ciencias Físicas y Matemáticas, Universidad de Chile, Santiago, Chile

JOSÉ A. RUTLLANT

Centro de Estudios Avanzados en Zonas Aridas, La Serena, and Departamento de Geofísica, Facultad de Ciencias Físicas y Matemáticas, Universidad de Chile, Santiago, Chile

(Manuscript received 19 April 2014, in final form 24 December 2014)

ABSTRACT

Biological productivity in the ocean along the Chilean coast is tied to upwelling that is primarily forced by equatorward wind stress and wind stress curl on the ocean surface. Southerly alongshore flow is driven by the southeast Pacific (SEP) anticyclone, and its intensity and position vary on a range of time scales. Variability of the SEP anticyclone has been linked to large-scale circulations such as El Niño–Southern Oscillation and the Madden–Julian oscillation. The actual timing, duration, and nature of the seasonal meridional drift of the SEP anticyclone are associated with the onset, demise, and strength of the local upwelling season. Seasonal variation is especially marked at the Punta Lavapié (37°S) upwelling focus, where there is a clear upwelling season associated with a change of the cumulative upwelling index (CUI) slope between positive and negative. The Punta Lengua de Vaca (30°S) focus typically exhibits upwelling year-round and has less distinct transitions, making it more difficult to identify an enhanced upwelling season. A two-phase linear regression model, which is typically used to detect subtle climate changes, is applied here to detect seasonal changes in CUI at Punta Lengua de Vaca. This method objectively finds distinct transitions for most years. The spring-to-summer transition is more readily detected and the slackening of the upwelling-favorable winds, warmer waters, and longer wind strengthening–relaxation cycles change the coastal upwelling ecosystem. While the spring-to-summer transition at Punta Lengua de Vaca could be influenced by large-scale circulations, the actual dates of transition are highly variable and do not show a clear relationship.

1. Introduction

Seasonal changes of the subtropical eastern boundary upwelling system greatly influence the oceanic ecosystem. Southerly wind (from the south) along the coast of Chile is driven by the southeast Pacific (SEP) anticyclone, which is particularly strong in the austral spring and summer. The low-level wind exerts an equatorward wind stress and wind stress curl on the ocean surface close to shore that contributes to the upwelling of cool, nutrient-rich water from below, which is typically associated with enhanced biological productivity. Changes in the timing and strength of seasonal environmental factors in marine ecosystems have been widely recognized to affect their functioning over a wide range of trophic levels (e.g., Kosro et al. 2006; Bograd et al. 2009; and references therein).

Marked seasonal variation of coastal upwelling is associated with the meridional migration of the Pacific high over the year (Fig. 1). The arrow in each panel indicates the position along the coast where the average meridional wind is zero. North of the arrow is southerly, upwelling-favorable wind. South of the arrow is northerly, downwelling-favorable wind. From May to August,

* Retired.

Corresponding author address: David A. Rahn, Atmospheric Science Program, Department of Geography, University of Kansas, 201 Lindley Hall, 1475 Jayhawk Blvd., Lawrence, KS 66045-7613.
E-mail: darahn@ku.edu

DOI: 10.1175/JPO-D-14-0073.1

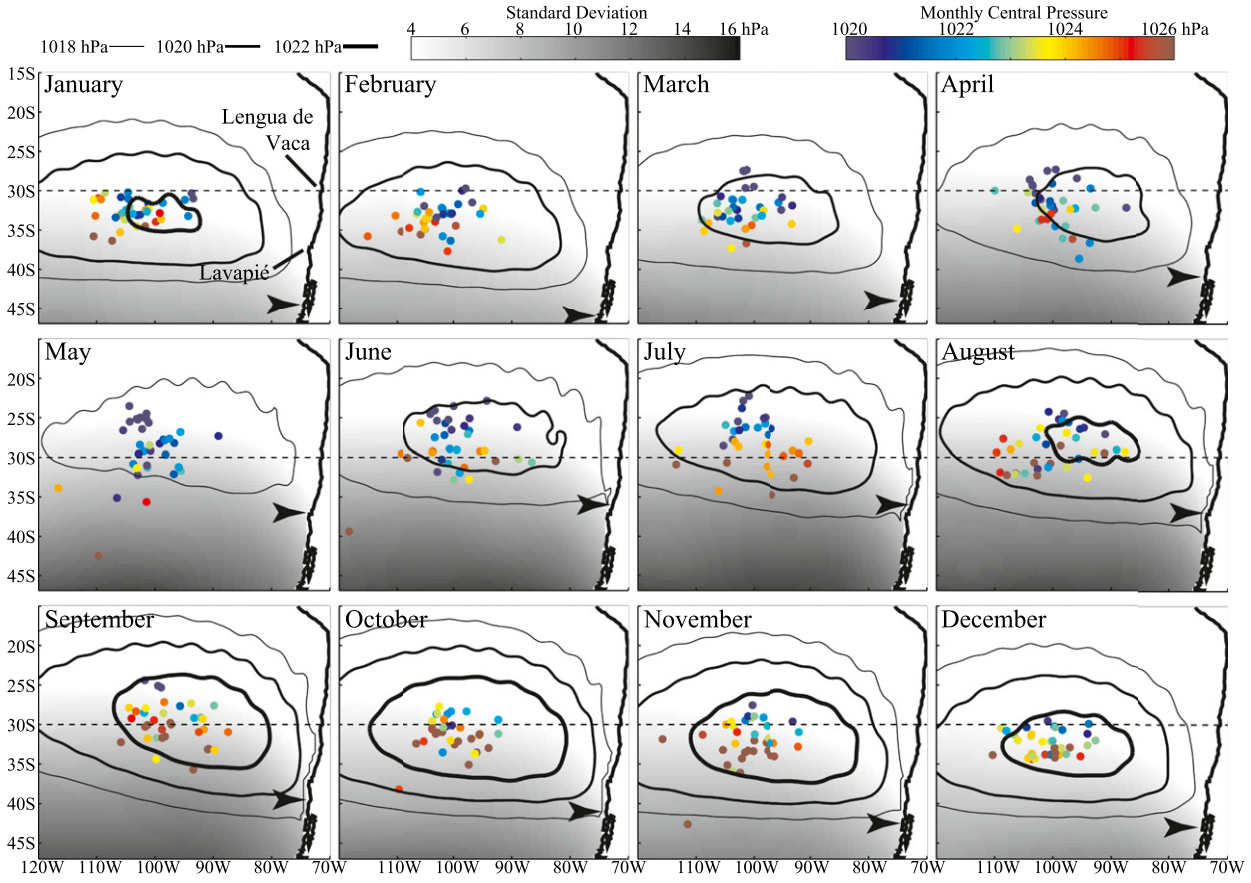

FIG. 1. Monthly average mean over 1979–2013 of sea level pressure (hPa; contours), magnitude and center position of the high pressure for each year (colored circles), standard deviation of mean sea level pressure (grayscale), and the location of the mean zero meridional wind at the coast is indicated by the large arrow. Data from the Climate Forecast System Reanalysis (Saha et al. 2010).

the arrow is at or north of Punta Lavapié (37°S), indicating a downwelling season. At other times of the year, the average wind is from the south and favors upwelling. Southerly wind driven by the synoptic conditions is enhanced by the topography such that a maximum in wind speed is present just downwind (north) of Punta Lavapié, one of the major upwelling foci along the coast of Chile (e.g., Garreaud and Muñoz 2005; Rahn and Garreaud 2014). Another location of strong upwelling-favorable wind is at Punta Lengua de Vaca (30°S), but it is evident that there the wind favors upwelling year-round. Even though there is upwelling year-round at Punta Lengua de Vaca, there is a period of enhanced upwelling in the austral spring and a slackening in the austral summer. Austral spring is September, October, and November. Austral winter is December, January, and February. Further references to seasons are all austral.

While the above discussion focuses on the long-term average, quasi-weekly cycles of strengthening and relaxation of upwelling-favorable winds happen in connection with coastal wind jets and coastal lows (e.g., Garreaud et al. 2002; Garreaud and Rutllant 2003; Rutllant 2004), which are weak and occasionally discernible at lower latitudes [e.g., at 23°S in Rutllant et al. (1998)]. Around 30°S coastal lows, propagating southward along the coast, gradually increase their frequency and seasonality southward into the zone dominated by the midlatitude, synoptic-scale storms of the west wind belt where downwelling dominates (e.g., Strub et al. 1998). This is represented in Fig. 1 by the higher standard deviation of the mean sea level pressure toward the south.

Ultimately, the seasonal signal in upwelling along the coast of Chile is associated with the annual swing in the strength and position of the SEP anticyclone. After reaching its northernmost position in July, the SEP anticyclone begins to strengthen and slowly shift southward in August. This continues over the next several months and as a result there is a greater alongshore pressure gradient force near the coast that drives stronger southerly winds. Then from January to March the anticyclone weakens but continues to move farther south. It remains weak and migrates northward from April to July.

There are various ways to assess upwelling seasons (e.g., Bylhouwer et al. 2013), but a common method for midlatitude regions is by using a cumulative upwelling index (CUI; e.g., Schwing et al. 2006). The CUI is a summation of a daily upwelling index over a period of time. The CUI can be defined several ways including alongshore wind stress, offshore surface Ekman transport, or pseudostress as used here, which is explained in the next section. The CUI is a popular quantity used to examine coastal upwelling. For example, Bograd et al. (2009) used a CUI at various points along the coast of California to determine several important dates including the spring transition, the peak seasonal upwelling, and the end of the upwelling season. Detection of the beginning and end of the upwelling season were found when the slope of CUI switched between positive and negative. Montecinos and Gomez (2010) used a similar technique by calculating the cumulative zonal Ekman transport near Punta Lavapié. Transitions were again defined when the slope changed between positive and negative. A clear influence of the El Niño–Southern Oscillation (ENSO) on the beginning and end of the upwelling season was shown at Punta Lavapié.

Identification of the start and end of the season is straightforward when there is both an upwelling and also a downwelling season. In contrast, at Punta Lengua de Vaca the upwelling may occur year-round, and the straightforward method of detecting the change in the upwelling slope from positive to negative is not sufficient to mark transitions in upwelling seasons. While the detection of the transition in upwelling is often blatantly clear at Punta Lavapié, it is not always as obvious at Punta Lengua de Vaca (30°S).

Even though the transition into and out of the enhanced upwelling season at Punta Lengua de Vaca is not as marked as Punta Lavapié, the implications for the upwelling and ecosystem are appreciable (Garreaud et al. 2011; Rutllant et al. 2013). During the Chilean Upwelling Experiment (CUpEx), time–depth plots of ocean temperature near the Punta Lengua de Vaca upwelling focus showed a clear response of the ocean temperature to a slackening of the wind at the end of the enhanced upwelling season (cf. Fig. 9 in Garreaud et al. 2011). Sea surface temperature increased about 1.5°C after the transition, but equally important is that the stability of the column increased noticeably as well. Stability in the top 50–100 m shifted from neutral to about 1°–1.5°C. Variability of the phytoplankton has been shown to be tied directly to the characteristics of the mixed layer (e.g., Echevin et al. 2008). Satellite-observed phytoplankton variability relative to the transition from a well-mixed ocean surface layer during the enhanced upwelling season (spring) to the more stratified surface layer after the spring-to-summer transition near the Punta Lengua de Vaca upwelling focus reveals larger variance of phytoplankton in the spring and smaller variance in the summer with similar low mean concentrations. At the corresponding upwelling shadow area (Tongoy Bay) where phytoplankton concentrations are significantly larger than in the focus, higher means and variances are observed in spring than in the summer (Rutllant et al. 2013). On the other hand, dominant species relative to the extremes of the ENSO cycle were reported in Rutllant and Montecino (2002). During the 1987 El Niño field experiment when a mean deeper thermocline and the presence of surface subtropical waters allowed for a more stratified surface layer, *Leptocylindrus sp.* dominated. Conversely, during the 1988 La Niña experiment, *Skeletonema sp.* were more abundant. The same type of shift in phytoplankton species have been reported before (La Niña like) and after (El Niño like) seasonal transitions studied here (Rutllant et al. 2013). Many factors influence the ecosystem, and all of them must be considered when explaining the final biological response. Additional factors include preconditioning from the previous winter, light levels, phenology of the biological components (e.g., grazers vs predators), and turbulent mixing. Performing a comprehensive examination of the biological response to the seasonal transition in wind is beyond the scope of this paper.

Fundamental questions regarding long-term changes to the upwelling or those forced by phenomena such as ENSO and the Madden–Julian oscillation (MJO) require an objective method to determine the dates of the enhanced upwelling season. There are two objectives of this paper: The first one is to present and explore an objective method based on well-established statistical methods, which are modified, and the interpretation is slightly different for this specific application. The second objective is to apply this method to examine the impact, if any, of ENSO and MJO on the transition date. Data are described in section 2. The basic method including underlying assumptions is outlined in section 3. An example of its application is given in section 4, and a summary is given in section 5.

2. Data and CUI

Two sets of reanalysis data are used. Both have a 0.5° grid spacing, and data are available every 6 h from 1979 to the present. Daily averages are computed as the average of the 0-, 6-, 12-, and 18-h values. The first reanalysis is the Climate Forecast System Reanalysis (CFSR; Saha et al. 2010) from the National Centers for Environmental Prediction (NCEP). The second reanalysis is the ERA-Interim (Dee et al. 2011) produced by the

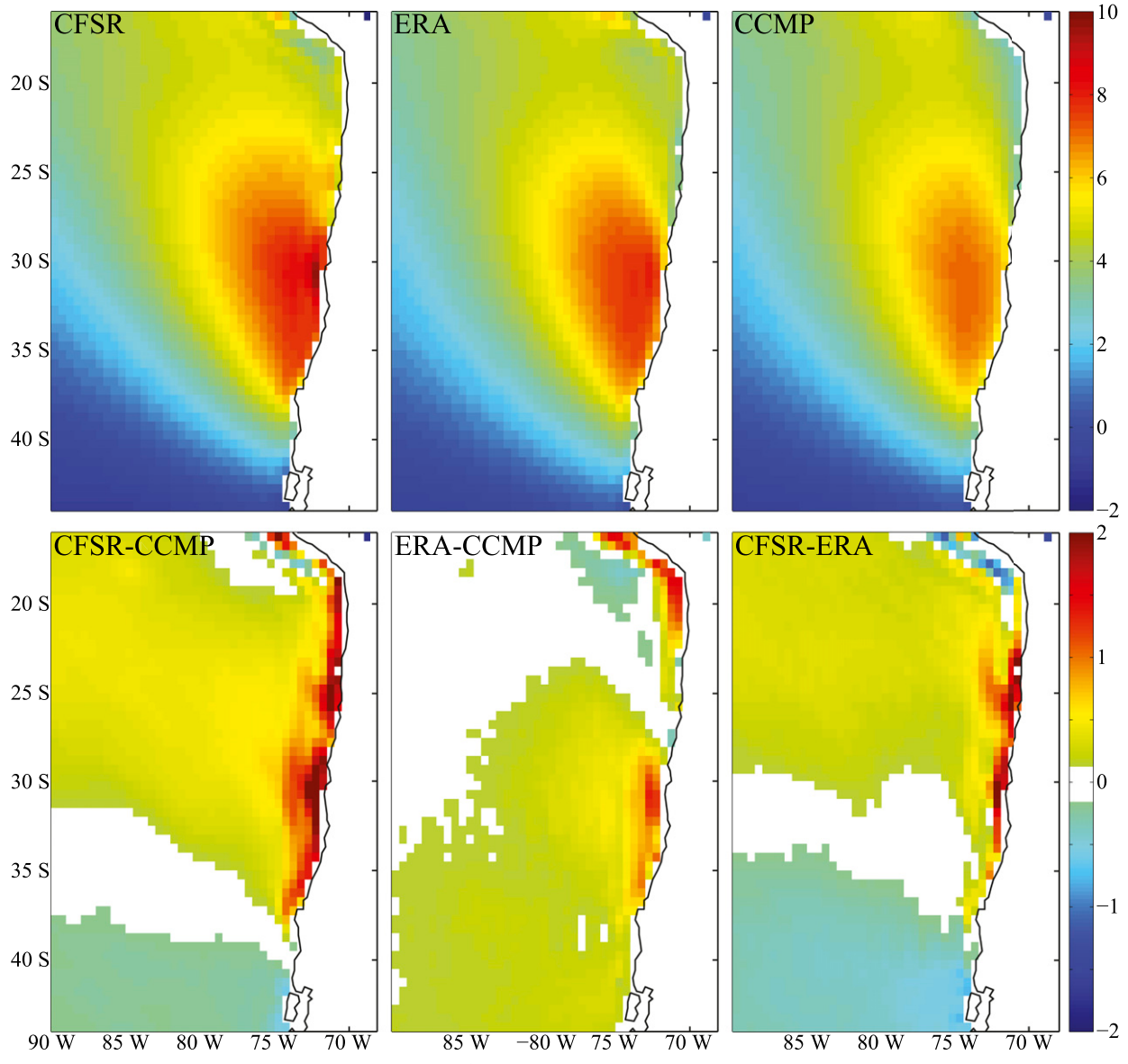

FIG. 2. (top) Average 10-m meridional wind speed ($m\,s^{-1}$) for November through January during the CCMP time period (1988–2010) for CFSR, ERA, and CCMP. (bottom) Difference between the different datasets as indicated in each panel.

European Centre for Medium-Range Weather Forecasts (ECMWF). Since the coastline is roughly north and south, the meridional component of the 10-m wind (v10) represents the alongshore flow. The grid point used to calculate the meridional wind at Punta Lengua de Vaca is at 30°S, 72°W. Both reanalyses have finer resolutions available, but 0.5° is the smallest grid spacing that they both have in common. As another reference, the cross-calibrated, multiplatform (CCMP) ocean surface wind velocity is used (Atlas et al. 2011). This dataset blends all available data from Remote Sensing Systems with conventional ship and buoy data and ECMWF analyses. Level 3.0 data are used, which are on a 0.25° grid and available every 6 h from 1987 to 2011.

Since much focus will be placed on the November–January timeframe, a comparison between the average meridional winds for all years during those 3 months is given in Fig. 2. The qualitative structure is the same between the datasets, but calculating the difference reveals that there are some biases up to $2\,m\,s^{-1}$ in some locations near the coast. While there is a bias between the datasets near the coast, it will be shown that the identification of the transitions using the CUI is not as heavily impacted by a bias that is on average higher or

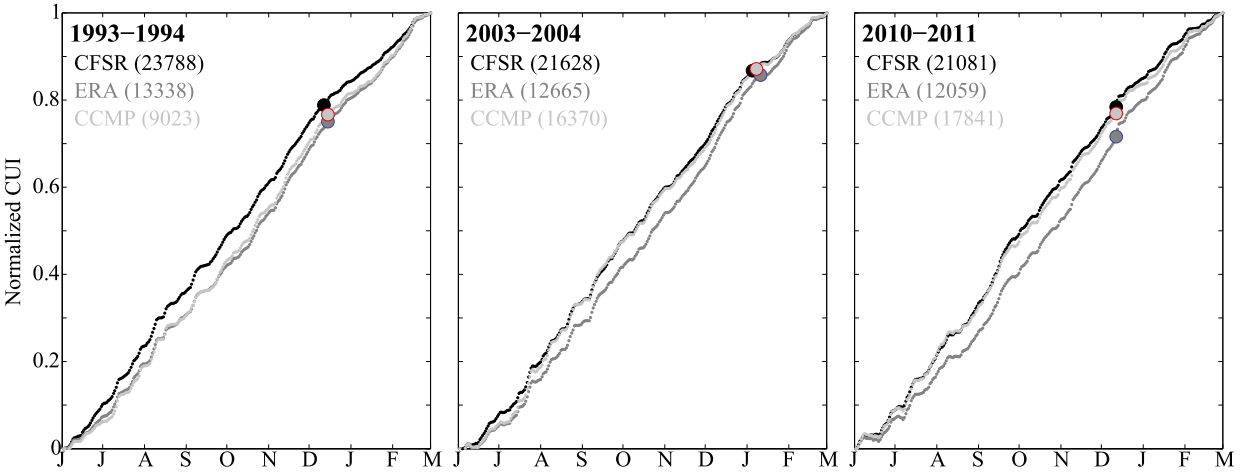

FIG. 3. Examples of the CUI normalized by the value at 1 Mar for each data source near Punta Lengua de Vaca at 30°S, 72°W for CFSR (black), ERA-Interim (gray), and CCMP (light gray). Normalized values are indicated by the corresponding data source in each panel.

lower than other datasets since it is the variability that is important for determining seasonal transitions. As long as changes to the slope of CUI exist, the actual value is not as important.

Before any method of detection is applied, the first step is to determine the CUI. A simple pseudowind stress is used to calculate the CUI. The pseudowind stress is a product of the alongshore (meridional) wind component and the wind speed (v10 × V10). The time period used is 1 June–1 March. A comparison of the CUI between the reanalysis data is performed to assess the differences between the datasets, and examples from 3 yr are given in Fig. 3. Because each dataset has a bias that impacts the magnitude of the CUI, the CUI is simply normalized by dividing each CUI by the value at 1 March so that they are all on the same scale. After normalizing, it becomes clear that the transitions and changes to the CUI are consistent between the three datasets, regardless of the average bias. Differences are still present, but for the purpose of detecting shifts in the slope, the data from each source depict the same trends and changes of slope.

3. Method

To objectively distinguish the subtle CUI changes in slope at Punta Lengua de Vaca, a two-phase linear regression model is applied. This type of statistical model has been used in a variety of climate applications [see Lund and Reeves (2002) and references therein]. The model is formulated here following Solow (1987):

$$X_t = \begin{cases} a_1 + b_1 t + e_t & 1 \le t \le c \\ a_2 + b_2 t + e_t & c < t \le n \end{cases}. \qquad (1)$$

Note that this model allows for both changes in intercept (step-type change) and also changes to the slope (trend type) phase changes. So, the changepoint (c) can represent step-type and/or trend-type phase changes. If there is a seasonal transition in CUI, then the changepoint will represent the date of the transition.

Before continuing, the fundamental assumptions of the linear regression model need to be made clear. These assumptions are that the linear model is correct and that the noise terms are independent, normally distributed around zero, and have a constant variance. From the examples of CUI in Fig. 3, strict adherence to these assumptions is questionable. These issues are identified now to be clear with the method and will be addressed when the method is applied.

The first issue is that after examining the slope of the line over the entire period, the slope is not particularly linear. There is also not necessarily one abrupt change to the slope, but multiple changes may exist. In Fig. 3, the 1993/94 CUI generally adheres to the underlying assumptions over a shorter time frame: October through mid-January. Before and after about a mid-December changepoint, the CUI is fairly linear. However, the whole time series exhibits other nonlinear characteristics and multiple changepoints, which can be identified in other years as well.

The second issue is that the noise terms are independent, normally distributed, and have a constant variance. Because this is a time series of meteorological data, there is autocorrelation in the noise terms so they are not truly independent. A constant variance is also not likely. A physical explanation for nonconstant variance is that during the winter there is typically more variance because of the passage of midlatitude cyclones, while there is much less activity during the spring and

summer when the SEP anticyclone is well established. This would contribute to a change of variance from one time of year to another. However, around the end of the upwelling season during November–January the variance in mean sea level pressure, and thus the wind that the pressure distribution forces, is typically small at 30°S (Fig. 1). More variance exists at the beginning of the upwelling season, which explains why changepoints are more difficult to detect at the beginning of the upwelling season than at the end.

To detect if there is a changepoint, several steps must be taken. First, the two-phase linear model has to be significantly better than applying a single linear regression. A significance test is constructed where the null hypothesis is the single linear regression and the alternative hypothesis is the two-phase linear regression. Since the location of the changepoint is unknown, this test must be performed at every point t in the time series. The first and last five points in the time series are not tested because of edge effects. To find the most likely changepoint, it is where the likelihood ratio statistic (F) is the greatest. Just because there is a significant difference between one and two linear regressions does not mean that it is a changepoint; the changepoint is where F is a maximum.

The likelihood ratio statistic is

$$F = \frac{S_o - S}{3} \Big/ \frac{S}{n-4}, \tag{2}$$

where S is the residual sum of squares from the alternative model (1), and S_o is the residual sum of squares from fitting the null hypothesis of a single linear regression:

$$X_t = a_1 + b_1 t + e_t, 1 \le t \le n. \tag{3}$$

The maximum value of F over the time series is the most likely changepoint. If there is a significant changepoint at time t, then F should be too large to attribute to random variation. The threshold of statistical significance comes from finding the distribution of F under the null hypothesis. Lund and Reeves (2002) have argued that prior use of the F distribution with 3 degrees of freedom in the numerator and $n - 4$ degrees of freedom in the denominator ($F_{3,n-4}$) is incorrect because of the dependence of the series and leads to overestimation of significant changepoints. They use a Monte Carlo approach to estimate the critical values. As will become clear later on, this distinction does not impact the findings in this case since the values of F are so large.

This model also assumes that there is only one changepoint in the series. To find the most prominent changepoint, it is estimated from the maximum F of the series. However, there could be more than one changepoint in the series. Lund and Reeves (2002) suggest finding the most prominent changepoint, eliminating it by adjusting the series, and then successively test for other changepoints in the same manner. A different method will be used here.

Employing the technique over the entire period from 1 June to 1 March is not valid since the long time scale does not conform well to the assumptions (linear model and noise term). Shorter time periods are generally more linear and fit the two-phase model better, although still not perfect. The reasoning behind this is that the wind strength is similar during a particular season and changes with season. To use shorter time frames but still cover the entire period from 1 June to 1 March, the method was repeated in a 90-day window centered on each day. The F statistic for each window was saved, and the maximum F statistics for all windows was used to identify the major changepoints over the entire time period. Windows with a different time span were used to test the impact of longer or shorter periods, but the 90-day window was found to be optimal in detecting the seasonal transition. Longer windows tend to have flatter F statistics. Shorter windows have more peaks that are influenced too much by synoptic-scale variability and do not capture the seasonal transitions as well as the 90-day window.

To summarize, the following steps are taken for each year:

1) Calculate the likelihood ratio statistic (F statistic) at each point in the first 90-day window.
2) Repeat step 1 for each 90-day window.
3) Find the maximum F statistic for each day over all 90-day windows.
4) Use the maximum F statistic for each day to find the local maximum of F that represents the most likely changepoint.

4. Results

a. *Application of method*

For brevity, not all 34 seasons will be shown and only the CUI from CFSR is plotted since the different datasets give similar results (usually yielding transitions within a few days of each other). Figure 4 depicts the CUI and F statistic for several representative years. Except for brief periods of a negative CUI slope associated with transient synoptic features, it is clear that upwelling exists year-round, but there is a period of enhanced upwelling in the spring. The distribution of F for all 90-day windows is shown by the thin gray lines;

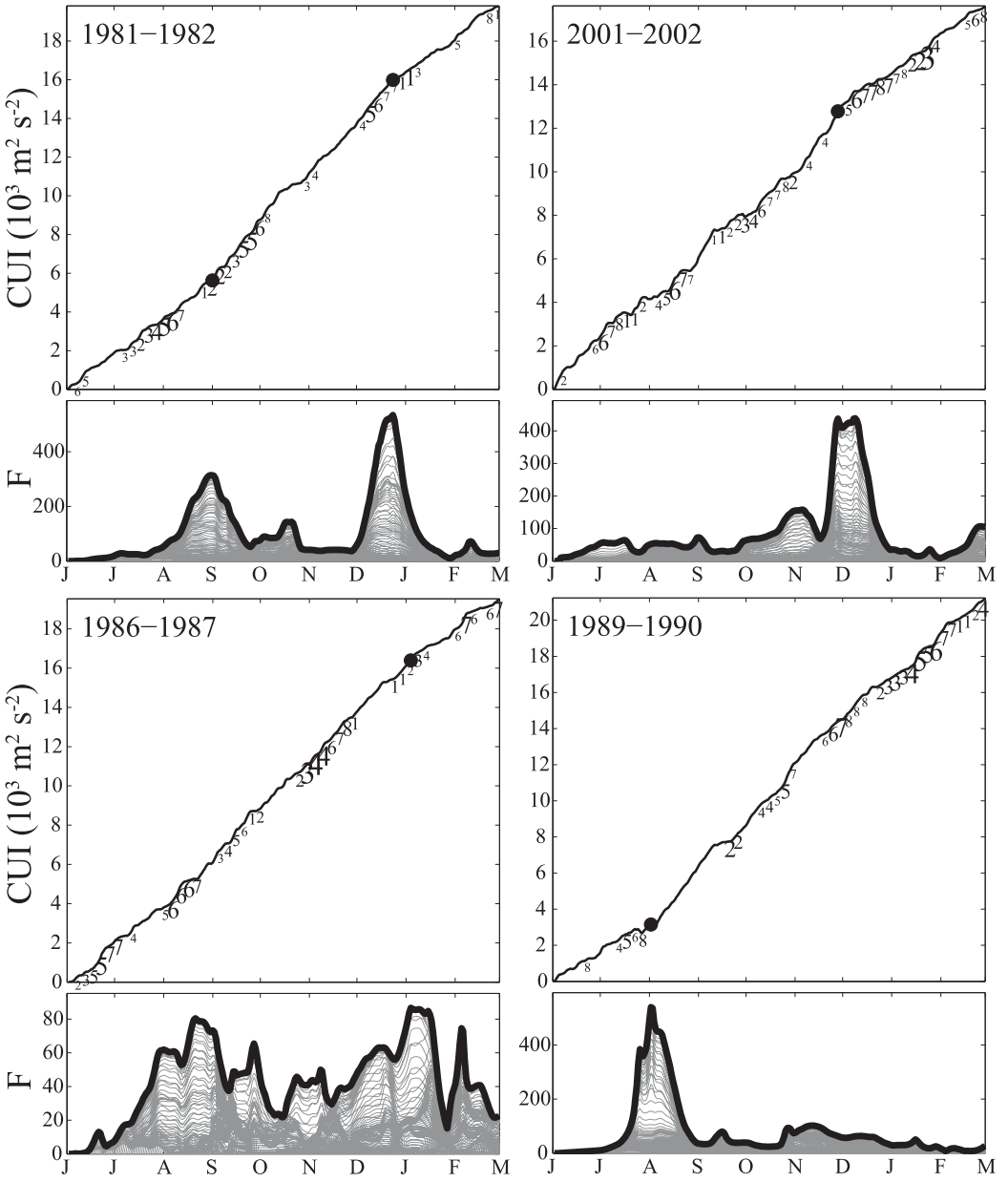

FIG. 4. Four examples of CUI and associated values of *F*. Numbers underneath CUI are the phase of the MJO, and the relative size of the number is the relative magnitude. Only phases when MJO > 1 are plotted. Thin gray lines are *F* for every 90-day window, and the bold line is the maximum *F* of all windows. The years are indicated in each panel.

the maximum *F* of all windows is the bold black line. Peaks correspond to the most prominent changepoints and thus the most likely time of the transition between enhanced and diminished upwelling seasons at Punta Lengua de Vaca. This method reveals many years that have a clear transition as the CUI slackens around December. The 1981/82 season is one example of the most frequently occurring type of time series of the CUI. There is a fairly well-defined start of the enhanced upwelling season just before September, and it slackens just before January.

Seasonal transitions are usually easy to identify from *F* since they correspond to the maximum value in the peak, in particular during the spring-to-summer transition. However, a few years such as 2001/02 do not have one single, sharp peak. If the peak is flat then there is a range of dates that could be selected. The fairly flat peak in 2001/02 spans 11 days. The small range of dates

adds some noise to the method because of a lack of sharpness. This could be dealt with in a couple ways. If the peak is flat then the transition date could be identified as the first point at approximately the same value. In this work, we identify the transition date as the numerical maximum of that peak. Also during the 2001/02 season, no clear beginning to the enhanced upwelling season is identified using this method. A lot of variability tends to flatten the F statistic, which indicates that no clear signal can be pulled out of the CUI.

Often the two-phase linear regression model is used to detect subtle changes in time series data (Lund and Reeves 2002). It quickly becomes obvious that the CUI undergoes large changes in both slope and intercept, even in 90-day windows. As a result, tests for statistical significance of the changepoints reveal that almost all points are significant changepoints. When applying either Monte Carlo techniques or using $F_{3,n-4}$, the critical F value is around 6. Since the magnitude at the peaks is typically much larger, this is well above any test for significance. The application of this method is to primarily find just where the greatest changepoint is and not where significant changepoints occur, which is what this method is commonly used for when looking at climate records, for example.

Depending partly on the variability of CUI, there can be numerous peaks. An example is the 1986/87 season where several peaks of all roughly the same magnitude occur. This may also lead to some ambiguity. When there are numerous peaks, not only is the maximum magnitude important to identify the transition date, but the type of transition is also important (i.e., an increase or decrease to the slope). Finally, there were 5 yr where the method failed to detect any clear transition between spring and summer in data from the CFSR. The 1989/90 season is shown in Fig. 4. The method does not indicate a clear transition date of the CUI since there is no corresponding signal in F. There is some subjectivity to when the transition is clear or not using the F statistic, but we found that a value of 50 between the local maxima and nearby minima gave a reasonable indication of whether the transition was clear or not. More strict or relaxed criteria may be used.

A failure to detect a clear transition can be viewed as a simple failure of the method to detect any seasonal transition or that there was actually no abrupt shift but a rather smooth seasonal shift in the upwelling strength. Seasonal transitions of the California Current System have also been noted by Schwing et al. (2006) to be either gradual or unclear in some years. It is clear that there still is a transition into and out of a period of enhanced upwelling; the method is just not able to identify a specific date of this transition because the changes are gradual. We emphasize that for the years where no transition date is detected this does not mean that there is no enhanced upwelling season. It means that this method just does not detect a clear transition date. However, we point out that most cases do have a distinct transition date that is readily detected by this method.

b. *Transition date*

Transition dates for the beginning and end of the enhanced upwelling season at Punta Lengua de Vaca are given in Table 1, which includes data from CFSR, ERA, and CCMP. Since CFSR and ERA cover the time period from 1979 to 2012 and CCMP data spans from 1988 to 2010, mean and standard deviation are calculated by averaging the dates over both time periods. The range of average start dates is from 31 August to 5 September. The range of average end dates is from 15 to 23 December. Furthermore, there is a clear difference in the standard deviation of the transition dates such that the beginning transition has a range of 22–30 days, while the standard deviation of the end dates is 12–17 days.

Another method to find the mean transition dates was to average the CUI over all years and then perform the above method on the average CUI to detect any changepoints. Figure 5 shows the results using all three datasets over just the CCMP time period (1988–2010). While the magnitude of the F statistic varies, the location of the peaks is in agreement. A large peak at the end of the enhanced upwelling season is clear and sharp in all datasets. The peak at the beginning of the enhanced upwelling season is present but broader and much less prominent. The higher standard deviation at the beginning of the enhanced upwelling season broadens the peak, and this is again attributed to the higher synoptic variability during this time of year. This is similar to the large variability of the onset of the upwelling season between northern California and Vancouver Island found by Bylhouwer et al. (2013). The smaller variability during the spring-to-summer transition results in a much sharper peak. The range of average transition dates for the 1988–2010 subset is 7–9 September and 8–10 December. The spring-to-summer transition found this way is earlier than that found by just taking the average of dates (15–21 December). Using the full dataset of CFSR and ERA (1979–2012) to calculate the mean, the transitions occur on 18 and 20 December, which is more in agreement with calculating the mean from the transition dates.

Because of the fairly large standard deviation of the transition, an explanation for why some years were earlier or later than others was sought. At Punta Lavapié, ENSO was shown by Montecinos and Gomez (2010) to exert a large influence on the start and end

TABLE 1. Dates of the start and end of the enhanced upwelling season and the duration (days) of the enhanced upwelling season obtained from CFSR, ERA, and CCMP.

	Start			End			Duration		
Year	CFSR	ERA	CCMP	CFSR	ERA	CCMP	CFSR	ERA	CCMP
1979	30 Jul	29 Jul		8 Jan	7 Jan		162	162	
1980	3 Aug	2 Aug		4 Jan	16 Jan		154	167	
1981	1 Sep	30 Aug		24 Dec	20 Dec		114	112	
1982	30 Sep	29 Sep		25 Dec	25 Dec		86	87	
1983	—	—		21 Nov	26 Nov		—	—	
1984	4 Oct	3 Oct		16 Dec	14 Dec		73	72	
1985	5 Aug	3 Aug		—	—		—	—	
1986	—	—		4 Jan	4 Jan		—	—	
1987	16 Aug	15 Aug		21 Jan	22 Jan		158	160	
1988	26 Aug	26 Aug	25 Aug	26 Dec	2 Jan	2 Jan	122	129	130
1989	2 Aug	2 Aug	2 Aug	—	—	—	—	—	—
1990	—	—	9 Sep	—	—	—	—	—	—
1991	16 Oct	17 Oct	17 Oct	14 Dec	18 Dec	8 Jan	59	62	83
1992	11 Sep	12 Sep	11 Sep	26 Dec	1 Jan	31 Dec	106	111	111
1993	—	—	—	10 Dec	15 Dec	15 Dec	—	—	—
1994	13 Aug	13 Aug	13 Aug	—	—	—	—	—	—
1995	—	—	—	28 Nov	28 Nov	25 Nov	—	—	—
1996	3 Sep	3 Sep	4 Sep	25 Nov	26 Nov	26 Nov	83	84	83
1997	16 Aug	17 Aug	16 Aug	12 Dec	16 Dec	16 Dec	118	121	122
1998	26 Sep	26 Sep	27 Sep	11 Jan	9 Jan	7 Jan	107	105	102
1999	—	14 Sep	—	—	—	—	—	—	—
2000	19 Sep	19 Sep	19 Sep	6 Dec	7 Dec	7 Dec	78	79	79
2001	—	—	—	9 Dec	10 Dec	10 Dec	—	—	—
2002	6 Sep	5 Sep	26 Aug	1 Dec	3 Dec	3 Dec	86	89	99
2003	21 Jul	8 Sep	14 Sep	27 Dec	11 Jan	30 Dec	159	125	107
2004	20 Aug	20 Aug	19 Aug	26 Dec	7 Jan	14 Jan	128	140	148
2005	13 Oct	13 Oct	14 Oct	11 Dec	6 Dec	12 Dec	59	54	59
2006	29 Aug	29 Aug	29 Aug	5 Jan	13 Dec	6 Jan	129	137	130
2007	—	—	—	7 Dec	8 Dec	6 Dec	—	—	—
2008	29 Jul	30 Jul	3 Aug	3 Dec	—	—	127	—	—
2009	31 Aug	31 Aug	—	31 Dec	11 Jan	22 Jan	122	133	—
2010	26 Sep	26 Sep	26 Sep	12 Dec	12 Dec	12 Dec	77	77	77
2011	8 Sep	10 Sep		12 Dec	22 Dec		95	103	
2012	—	—		26 Dec	27 Dec		—	—	
Mean [standard deviation (days)]									
1988 to 2010	1 Sep (30)	5 Sep (22)	5 Sep (23)	15 Dec (12)	20 Dec (17)	21 Dec (17)	104 (29)	103 (29)	102 (26)
1979 to 2012	31 Aug (25)	31 Aug (23)	—	19 Dec (16)	23 Dec (17)	—	109 (32)	110 (33)	—

of the upwelling season. The date of the spring-to-summer transitions at Punta Lengua de Vaca is grouped according to the phase of ENSO in November–December–January. The specific ENSO index used was the Oceanic Niño index available from the Climate Prediction Center (www.cpc.ncep.noaa.gov/products/analysis_monitoring/ensostuff/ensoyears.shtml). The average spring-to-summer transition dates during El Niño, La Niña, and neutral conditions are 25 December, 11 December, and 23 December, respectively. The average of all dates was 19 December. To test for significance, a Welch's t test is used with the null hypothesis that the mean during La Niña and El Niño are equal. At an α level of 0.90, there is a statistically significant difference in the transition date between El Niño and La Niña years at Punta Lengua de Vaca. However, under the null hypothesizes that El Niño or La Niña are different than neutral years, there is no significant difference, which indicates a marginal influence of ENSO on the transition date at this particular location at an α level of 0.90.

The minor role, if any, that ENSO has on the seasonal transition of upwelling winds at this latitude is consistent with Montecinos (1991) who concluded that the equatorward winds are not clearly modulated by ENSO. Rahn (2012) also showed spring and summer composites

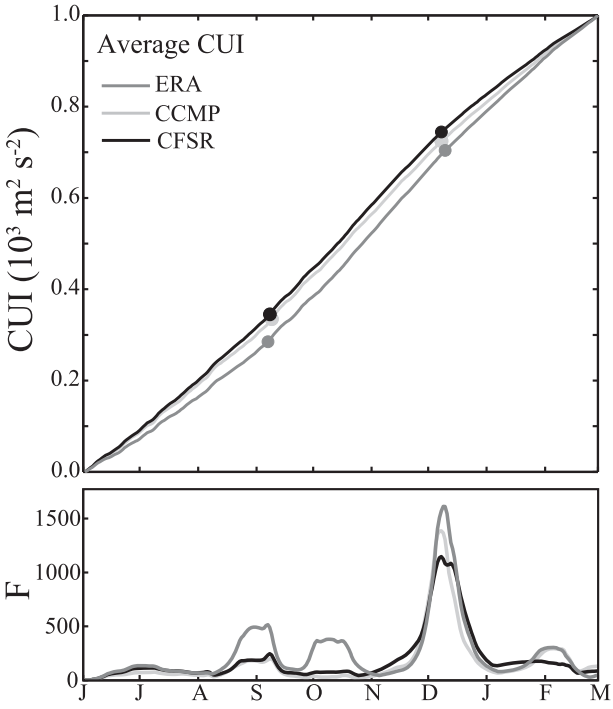

FIG. 5. (top) Average CUI over the CCMP period (1988–2010) with transition dates indicated by the circles. (bottom) Values of the maximum *F* from CFSR (black), ERA (gray), and CCMP (light gray).

of alongshore wind anomalies during ENSO that had no significant anomalies near Punta Lengua de Vaca. In the spring and summer (September to February) composites, there were anomalies to the north and south of Punta Lengua de Vaca. Since the spring-to-summer transition occurred during November to January, composites of the meridional wind anomaly are constructed for just those months (Fig. 6; positive anomalies indicate more equatorward wind). No significant anomaly was found during La Niña, but there was a significant positive anomaly found during El Niño. The positive anomaly found during El Niño is centered south of the mean center of the anticyclone (Fig. 1). In fact, most years that are associated with strong anticyclones tend to occur south of the mean location of the anticyclone. Enfield (1981) and later Vargas et al. (2007) argued that when the SEP anticyclone weakened during El Niño, there was a deeper MBL associated with reduced low cloud cover that increased the land–sea thermal contrast. They suggested that the greater temperature gradient would drive stronger equatorward wind near the coast and explain the stronger equatorward wind speed.

The MJO is an atmospheric oscillation around the equator that plays a role in modifying the regional circulation conditions along the coast of Chile (e.g., Barrett et al. 2012; Juliá et al. 2012). An active MJO represents the often irregular eastward propagation of a large area of convection along the equator with suppressed convection on either side. The speed of propagation around the globe results in a period typically in the range of 30–60 days. Distinct patterns of anomalies in the atmospheric circulation are associated with an active MJO and can modulate weather patterns globally through teleconnections (e.g., Donald et al. 2006). For instance, when the equatorial convection is centered over Indonesia the surface pressure over the SEP strengthens and the southerly wind along the Chilean coast is greater than normal. The Wheeler and Hendon (2004) index is a commonly used metric of the MJO that provides information on the phase and amplitude of the MJO. The phase of the MJO describes where the enhanced convection is located, and the amplitude indicates the magnitude of the anomalies associated with the MJO. When there is a large area of convection near Indonesia, the MJO is in phase 5. If the cluster of convection moves eastward until it reaches the international date line, then the phase is 7. When the MJO is in phase 7, the SEP anticyclone becomes weaker than normal. As the equatorial convection continues to propagate farther eastward through phase 8 and back to phase 1 the SEP anticyclone is on average weaker than normal and the southerly wind is also weaker. The opposite anomaly pattern is true for phases 4 and 5.

Composites over the entire year centered near Chile indicate phases 4, 5, and 6 (7, 8, and 1) of the MJO tend to have stronger (weaker) equatorward alongshore wind (Rahn 2012). To visualize the relationship between the alongshore wind and MJO during the spring-to-summer transition, only the statistically significant anomalies from November to January for each phase of the MJO with an amplitude more than one are shown (Fig. 7). Greatest anomalies of the composite reach $\pm 2\,\mathrm{m\,s^{-1}}$. The anomalies generally shift from north to south along the coast as the MJO progresses west to east along the equator (increasing phase number). Even though the greatest anomalies are found at Punta Lavapié, significant anomalies are also found farther north near Punta Lengua de Vaca.

Since one could expect a sharp change whenever the MJO progresses eastward from phases 4, 5, and 6 (southerlies strengthen) to phases 7, 8, and 1 (southerlies weaken), transitions modulated by the MJO should mostly occur over phases 5, 6, and 7. A histogram of the MJO phase at the date of the spring-to-summer transition indicates that the most common MJO phase is 6 or 7 (Fig. 8), consistent with the composites. However, transitions have occurred in all other phases, and many transitions occur when there is no significant MJO

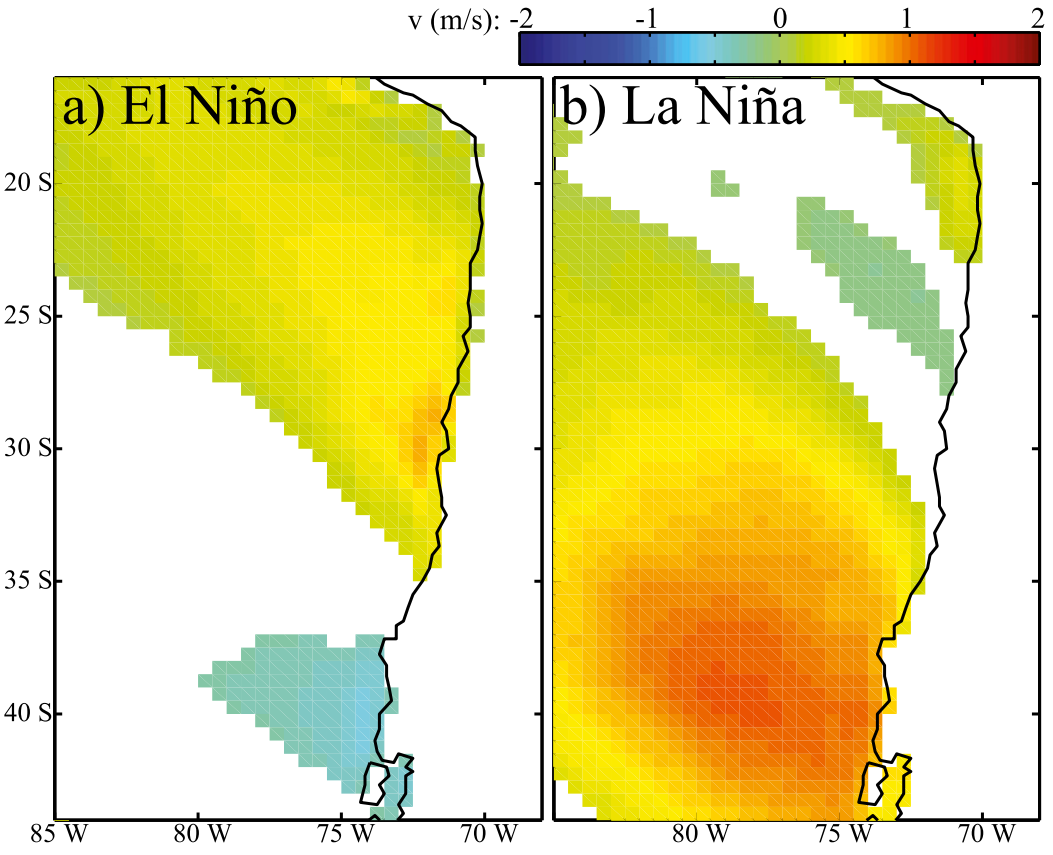

FIG. 6. Composites of significant 10-m meridional wind speed anomalies ($m\,s^{-1}$) during November, December, and January under (a) El Niño and (b) La Niña conditions. Data from the CFSR.

(amplitude < 1). Thus, it is concluded that the transition is more likely to happen during a significant MJO in phases 6 or 7, but by no means is the MJO a clear indicator of the transition date. Even though there appears to be a relationship with MJO and the spring-to-summer transition, there is still a considerable amount of variability. In fact, in the four examples of Fig. 3, none of the transitions occur during phase 6. So, even though it is slightly more likely to occur in phases 6 or 7, there is little to no predictability in the transition time period based off of just the phase of the MJO.

5. Conclusions

Determining the onset and end of the enhanced upwelling season is important for the functioning of the marine ecosystem. The enhanced upwelling season is tied to the SEP anticyclone that migrates north and south over the year and strengthens in the spring and summer months. Locations that are on the southern extent of the SEP anticyclone, such as near Punta Lavapié, have distinct transition points between the upwelling and downwelling seasons. Thus, seasonal transitions are readily identifiable. Farther north near Punta Lengua de Vaca, the average wind is southerly year-round, making identification of the enhanced upwelling season more difficult to assess.

An objective method to detect the more subtle changes in CUI near Punta Lengua de Vaca was developed and applied to three datasets to find the transition dates over the years 1979–2013. This method detects changepoints by essentially comparing a simple linear regression model to a two-phase linear regression model. The maximum difference corresponds to the most likely changepoint. The underlying assumptions in these models are that the time series is linear (one or two phase) and that the noise is independent, normally distributed, and has a constant variance. These assumptions are weak over the entire period but strengthen over shorter time periods. To use a shorter time period but cover the entire time series, this method was applied to all days in a 90-day window. Longer and shorter time periods were used, but the 90-day window tends to be ideal to capture the seasonal transition. Shorter time periods were influenced too much by synoptic systems

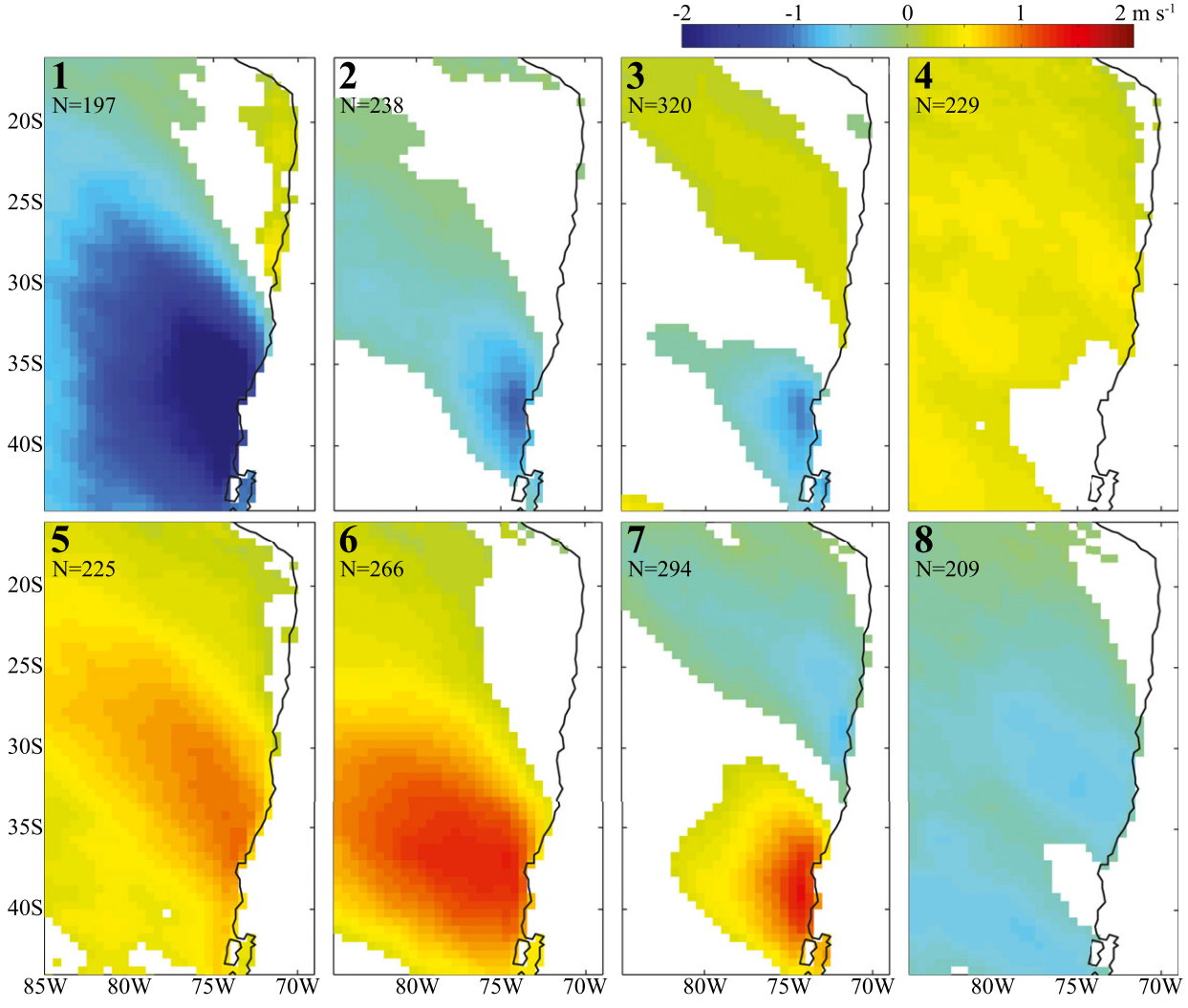

FIG. 7. Composites of significant 10-m meridional wind speed anomalies ($m\,s^{-1}$) during November, December, and January for each phase of the MJO (indicated in the upper-left panel) when amplitude is greater than one. The number of days (N) is indicated in each panel. Data from the CFSR.

and longer periods were less robust with the underlying assumptions.

The method could objectively identify clear transition points for most years. The failure to detect a change-point in those years with no clear transition is attributed to high variability and really no clear, sharp transition in CUI at the beginning or end of the enhanced upwelling period. Using all datasets, the average day of the start to the enhanced upwelling season ranged from 31 August to 5 September, while the end of the enhanced upwelling season ranged from 15 to 23 December. There is a higher standard deviation (22–30 days) for the initial transition date and a lower standard deviation (12–17 days) for the end date. The difference likely comes from more synoptic activity that occurs near the beginning of the enhanced upwelling season than at the end. We also hypothesize that the difference in the start and end of the enhanced upwelling season is influenced by the atmospheric semiannual oscillation in sea level pressure (e.g., Walland and Simmonds 1999). This is because the difference in the maximum meridional temperature gradient and rate of amplification of baroclinic waves changes greatly between the start and end of the enhanced upwelling season.

Explanations for the year-to-year changes in the transition date were sought. Unlike Punta Lavapié where ENSO plays a large role (Montecinos and Gomez 2010), the influence of ENSO on the meridional wind and CUI was minor at Punta Lengua de Vaca. The MJO can also contribute to modifying the seasonal transition.

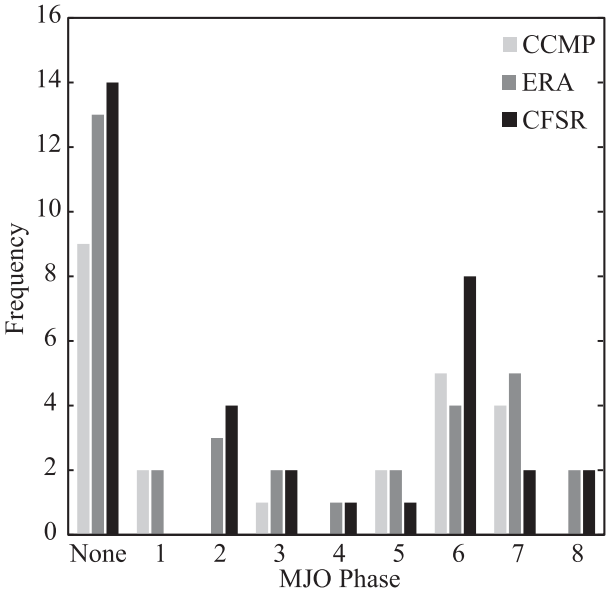

FIG. 8. Histogram of the phase of the MJO at the spring-to-summer transition date for CFSR (black), ERA (gray), and CCMP (light gray). None indicates a MJO amplitude that is less than 1 or no clear transition.

Composites of the meridional wind anomalies during November, December, and January reveal that there are significant anomalies near Punta Lengua de Vaca. A slackening of the wind was slightly more likely to occur when the MJO was in phase 6 or 7, but the transition also occurred in almost every other phase, and 14 transitions occurred with no active MJO (amplitude > 1) at all. Thus, the relationship of the MJO and transition date is not robust. As with any global teleconnection pattern, there are likely many factors that contribute to the transition date that makes it difficult to quantify a robust relationship to any one factor such as ENSO or the MJO.

Acknowledgments. We thank the three anonymous reviewers for their comments and suggestions that improved the manuscript, and we are grateful for the fruitful discussions with CEAZA's Marcel Ramos and Beatriz Yannicelli. Support for this work comes from New Faculty Startup funds at KU.

REFERENCES

Atlas, R., R. N. Hoffman, J. Ardizzone, S. M. Leidner, J. C. Jusem, D. K. Smith, and D. Gombos, 2011: A cross-calibrated, multiplatform ocean surface wind velocity product for meteorological and oceanographic applications. *Bull. Amer. Meteor. Soc.,* **92,** 157–174, doi:10.1175/2010BAMS2946.1.

Barrett, B. S., J. F. Carrasco, and A. P. Testino, 2012: Madden–Julian oscillation (MJO) modulation of atmospheric circulation and Chilean winter precipitation. *J. Climate,* **25,** 1678–1688, doi:10.1175/JCLI-D-11-00216.1.

Bograd, S. J., I. Schroeder, N. Sakar, X. Qiu, W. J. Sydeman, and F. B. Schwing, 2009: The phenology of coastal upwelling in the California Current. *Geophys. Res. Lett.,* **36,** L01602, doi:10.1029/2008GL035933.

Bylhouwer, B., D. Ianson, and K. Kohfeld, 2013: Changes in the onset and intensity of wind-driven upwelling and downwelling along the North American Pacific coast. *J. Geophys. Res. Oceans,* **118,** 2565–2580, doi:10.1002/jgrc.20194.

Dee, D. P., and Coauthors, 2011: The ERA-interim reanalysis: Configuration and performance of the data assimilation system. *Quart. J. Roy. Meteor. Soc.,* **137,** 553–597, doi:10.1002/qj.828.

Donald, A., H. Meinke, B. Power, A. De H. N. Maia, M. C. Wheeler, N. White, R. C. Stone, and J. Ribbe, 2006: Near-global impact of the Madden–Julian oscillation on rainfall. *Geophys. Res. Lett.,* **33,** L09704, doi:10.1029/2005GL025155.

Echevin, V., O. Aumont, J. Ledesma, and G. Flores, 2008: The seasonal cycle of surface chlorophyll in the Peruvian upwelling system: A modelling study. *Prog. Oceanogr.,* **79,** 167–176, doi:10.1016/j.pocean.2008.10.026.

Enfield, D. B., 1981: Thermally driven wind variability in the planetary boundary layer above Lima, Peru. *J. Geophys. Res.,* **86,** 2005–2016, doi:10.1029/JC086iC03p02005.

Garreaud, R., and J. Rutllant, 2003: Coastal lows in north-central Chile: Numerical simulation of a typical case. *Mon. Wea. Rev.,* **131,** 891–908, doi:10.1175/1520-0493(2003)131<0891:CLATSW>2.0.CO;2.

——, and R. Muñoz, 2005: The low-level jet off the subtropical west coast of South America: Structure and variability. *Mon. Wea. Rev.,* **133,** 2246–2261, doi:10.1175/MWR2972.1.

——, J. Rutllant, and H. Fuenzalida, 2002: Coastal lows in north-central Chile: Mean structure and evolution. *Mon. Wea. Rev.,* **130,** 75–88, doi:10.1175/1520-0493(2002)130<0075:CLATSW>2.0.CO;2.

——, ——, R. C. Muñoz, D. A. Rahn, M. Ramos, and D. Figueroa, 2011: VOCALS-CUpEx: The Chilean Upwelling Experiment. *Atmos. Chem. Phys.,* **11,** 2015–2029, doi:10.5194/acp-11-2015-2011.

Juliá, C., D. A. Rahn, and J. A. Rutllant, 2012: Assessing the influence of the MJO on strong precipitation events in subtropical, semi-arid north-central Chile (30°S). *J. Climate,* **25,** 7003–7013, doi:10.1175/JCLI-D-11-00679.1.

Kosro, P. M., W. T. Peterson, B. M. Hickey, R. K. Shearman, and S. D. Pierce, 2006: Physical versus biological spring transition: 2005. *Geophys. Res. Lett.,* **33,** L22S03, doi:10.1029/2006GL027072.

Lund, R., and J. Reeves, 2002: Detection of undocumented changepoints: A revision of the two-phase regression model. *J. Climate,* **15,** 2547–2554, doi:10.1175/1520-0442(2002)015<2547:DOUCAR>2.0.CO;2.

Montecinos, A., 1991: Efecto del fenómeno El Niño en los vientos favorables a la surgencia costera en la zona norte de Chile (Effect of El Niño on upwelling-favorable winds in the northern zone of Chile). M.S. thesis, School of Marine Sciences, Catholic University of Valparaiso, 143 pp.

——, and F. Gomez, 2010: ENSO modulation of the upwelling season off southern-central Chile. *Geophys. Res. Lett.,* **37,** L02708, doi:10.1029/2009GL041739.

Rahn, D. A., 2012: Influence of large scale oscillations on upwelling-favorable coastal wind off central Chile. *J. Geophys. Res.,* **117,** D19114, doi:10.1029/2012JD018016.

——, and R. D. Garreaud, 2014: A synoptic climatology of the near-surface wind along the west coast of South America. *Int. J. Climatol.,* **34,** 780–792, doi:10.1002/joc.3724.

Rutllant, J. A., 2004: A comparison of spring coastal upwelling off central Chile at the extremes of the 1996–1997 ENSO cycle. *Cont. Shelf Res.,* **24,** 773–787, doi:10.1016/j.csr.2004.02.005.

——, and V. Montecino, 2002: Multiscale upwelling forcing cycles and biological response off north-central Chile. *Rev. Chil. Hist. Nat.,* **75,** 149–164, doi:10.4067/S0716-078X2002000100020.

——, H. Fuenzalida, R. Torres, and D. Figueroa, 1998: Interacción océano-atmósfera-tierra en la Región de Antofagasta (Chile, 23°S): Experimento DICLIMA. *Rev. Chil. Hist. Nat.,* **71,** 405–427.

——, B. Yannicelli, M. Ramos, and D. A. Rahn, 2013: Spring-summer transition in the coastal upwelling regime off north-central Chile: 30°S. *Int. Symp. on Climate Variability and Change on Marine Resources and Fisheries in the South Pacific: Toward a South Pacific Integrated Ecosystems Studies (SPICES) Program,* Concepción, Chile, INPESCA AND IMAS, Book of Abstracts, 12.

Saha, S., and Coauthors, 2010: The NCEP Climate Forecast System Reanalysis. *Bull. Amer. Meteor. Soc.,* **91,** 1015–1057, doi:10.1175/2010BAMS3001.1.

Schwing, F. B., N. A. Bond, S. J. Bograd, T. Mitchell, M. A. Alexander, and N. Mantua, 2006: Delayed coastal upwelling along the U.S. West Coast in 2005: A historical perspective. *Geophys. Res. Lett.,* **33,** L22S01, doi:10.1029/2006GL026911.

Solow, A. R., 1987: Testing for climate change: An application of the two-phase regression model. *J. Climate Appl. Meteor.,* **26,** 1401–1405, doi:10.1175/1520-0450(1987)026<1401:TFCCAA>2.0.CO;2.

Strub, P. T., J. M. Mesias, V. Montecino, J. Rutllant, and S. Salinas, 1998: Coastal ocean circulation off western South America: Coastal segment (6, E). *The Global Coastal Ocean: Regional Studies and Syntheses,* A. R. Robinson and K. H. Brink, Eds., The Sea—Ideas and Observations on Progress in the Study of the Seas, Vol. 11, John Wiley and Sons, 273–313.

Vargas, G., S. Pantoja, J. A. Rutllant, C. B. Lange, and L. Ortlieb, 2007: Enhancement of coastal upwelling and interdecadal ENSO-like variability in the Peru-Chile Current since late 19th century. *Geophys. Res. Lett.,* **34,** L13607, doi:10.1029/2006GL028812.

Walland, D., and I. Simmonds, 1999: Baroclinicity, meridional temperature gradients, and the southern semiannual oscillation. *J. Climate,* **12,** 3376–3382, doi:10.1175/1520-0442(1999)012<3376:BMTGAT>2.0.CO;2.

Wheeler, M., and H. Hendon, 2004: An all-season real-time multivariate MJO index: Development of an index for monitoring and prediction. *Mon. Wea. Rev.,* **132,** 1917–1932, doi:10.1175/1520-0493(2004)132<1917:AARMMI>2.0.CO;2.